Connected-Element Interferometer Holography via Correlation of Signals from the Common Platform

Alberto Torre* and Manuel Vázquez*

ABSTRACT. — Microwave antenna holography is traditionally done in the Deep Space Network (DSN) with beacons coming from Ku-band geostationary satellites and a small 3-meter dish as reference antenna. This reports shows a new tool that has been integrated into the antenna calibration and measurement equipment (ACME) that allows making holographies at DSN frequency bands using other antennas from the complex as the reference. This tool is based on a software cross-correlator implemented in a graphics processing unit (GPU) that can process bandwidths up to 100 MHz. With this capacity, wideband signals from spacecrafts or radio stars can be used to perform the correlation. A signal model is developed and main system budgets are calculated. Finally, some actual measurements done with this new system are shown.

I. Introduction

Antenna microwave holography is a mature technique that has been used in the DSN for several decades in order to characterize with great precision several key parameters of the dish, such as panel alignment, subreflector position, and aperture ilumination [1]. The exisiting equipment to perform these holographies is based on a network analyzer that measures the phase difference of one beacon signal after being received by the reference antenna and the antenna under test (AUT). Due to the lack of strong beacons in spacecrafts at DSN frequency bands, holographies have been done with the beacons from geosynchronous satellites at Ku-band. These beacons are powerful enough to conduct high-resolution holographies, and have the advantage that the AUT barely moves in elevation during the measurement. However, the parameters of the antenna cannot be evaluated in the operating frequency bands of the DSN with this method. For instance, there is no information about the aperture illumination by the

*Madrid Deep Space Communications Complex

The research described in this publication was carried out by the Jet Propulsion Laboratory, California Institute of Technology, under a contract with the National Aeronautics and Space Administration.

X/Ka operational feed, which is a valuable information to know about the status of the optics alignment. Besides, a new provisional Ku-band feed must be installed at the AUT, and consequently, periodic measurements of the antennas cannot be done regularly.

Back in 1983, the microwave holography technique was performed by JPL with a real-time connected-element interferometer in the 64-meter antenna at Tidbinbilla [2]. The idea of connecting the interferometer to the DSN bands was found to be particularly attractive, as the tracking commitments of the stations are very heavy and using other frequency bands or metrology methods would be prohibitively disruptive. This experiment was conducted in S-band using a 34-m antenna as reference, and 12 MHz bandwidth of 3C273 as signal source. According to the authors of that paper, the results of the experiment showed that connected-element interferometry would allow regular performance monitoring of the antennas. Unfortunately, no wide-bandwidth correlator has been available to the DSN since then, and all subsequent holographies in the DSN have been made with Ku-band beacons from geostationary satellites.

Recently, the DSN modernized the distribution of the signals coming from the antennas to its signal processing centers by means of the Common Platform [3]. Now every signal coming from the antennas is digitized and made available to the receivers by means of a commercial 10 Gbit/sec ethernet switch. The closed-loop and open-loop receivers connect via a network card to this switch, and process bandwidths of up to 100 MHz inside field programmable gate arrays (FPGAs). Developing a wideband correlator in an FPGA is feasible, but it would take a considerable effort. Another possibility is using GPUs to make the computations. GPUs are excellent tools to perform parallelizable operations such as fast Fourier transforms (FFTs), filtering, and matrix operations, which are the most important ones involved in making a cross-correlator. The massive adoption of GPUs for artificial intelligence (AI) and machine learning means that a lot of computing libraries and developement tools are readily available to ease the development of GPU applications.

To assess the feasibility of making the cross-correlator with a GPU, several prototypes were built. First, in 2019, a 25 MHz single-channel synthesis filter bank was done in Labview with all the processing done in the central processing unit (CPU). This prototype served to test that the user datagram protocol (UDP) frames coming from the ethernet switch could be synchronized and the peripheral component interconnect (PCI) 3.0 bus of the computer was fast enough to send signals from the ethernet card (Mellanox ConnectX-3) to the CPU. Then in 2020, a 100 MHz single-channel synthesis filter bank was built with a Quadro P4000 GPU card. With a GPU usage close to 80%, this second prototype proved that the UDP multicast stream could be processed in real time in a workstation. Then, a 100 MHz 2-channel cross-correlator prototype was built in 2021 with a Mellanox ConnectX-5, an Nvidia RTX 3090, and a PCI 4.0 computer with an AMD EPYC Milan processor. This cross-correlator has been under developement and testing for 2022 and 2023 in several holography campaigns at Madrid Deep Space Communications Complex (MDSCC). The experiments carried

out show the same antenna surface maps as those done with the narrowband Ku-band legacy holography system.

Great emphasis has been placed during the development on the automation of all tasks. To facilite the automation, the cross-correlator has been integrated into ACME. As a result, a short setup time is required to start the holography, and there is no need to be at the antenna shelter. Holographies can be done at any ops workstation, and it is not required to directly interface the antenna servo or the angle encoders. Predicts files are used to move the antenna, and time stamp information is used to synchronize antenna angular positions with digitized signals. A 51×51 mid-resolution X-band holography can be done with proper training in 2 hours. This means that small slots in the scheduling can be used for getting holographies on a regular basis. The reference antenna can also be used for holography while tracking a spacecraft with strong signals such as the Mars Reconnaissance Orbiter (MRO) or Solar Terrestrial Relations Observatory (STEREO). Therefore, only the AUT will be required to be available, with the consequent reduction of required resources.

Next chapters will show the design of the cross-correlator and the main results obtained so far.

II. Signal Model

Suppose two antennas separated by a baseline vector $\boldsymbol{D}$ are looking at a source with a unit vector $\boldsymbol{s} = \boldsymbol{s_0} + \boldsymbol{\sigma}$ in a certain direction within the source, where $\boldsymbol{s_0}$ is the center direction of the source (Figure 1).

The geometric delay between the same phase front from direction $\boldsymbol{s}$ is given by [4]:

$$\tau_g(\boldsymbol{\sigma}) = \frac{\boldsymbol{D}\cdot\boldsymbol{s}}{c} = \tau_{g0} + \frac{\boldsymbol{D}\cdot\boldsymbol{\sigma}}{c} \tag{1}$$

where c is the speed of light and $\tau_{g0} = \frac{\boldsymbol{D}\cdot\boldsymbol{s_0}}{c}$ is the delay of the wave coming from the reference direction $\boldsymbol{s_0}$. The electric field intensities that arrive at the antennas are

$$\begin{aligned} e_{Aut}(\boldsymbol{\sigma}, t) &= e_{Ref}(\boldsymbol{\sigma}, t - \tau_g(\boldsymbol{\sigma})) \\ e_{Ref}(\boldsymbol{\sigma}, t) &= e(\boldsymbol{\sigma}, t) \end{aligned} \tag{2}$$

Therefore, their spectrums are

$$\begin{aligned} e_{Aut}(\boldsymbol{\sigma}, \omega) &= e_{Ref}(\boldsymbol{\sigma}, \omega)\, e^{-i\omega\tau_g(\boldsymbol{\sigma})} \\ e_{Ref}(\boldsymbol{\sigma}, \omega) &= e(\boldsymbol{\sigma}, \omega) \end{aligned} \tag{3}$$

The electric fields are converted to voltages in the antennas

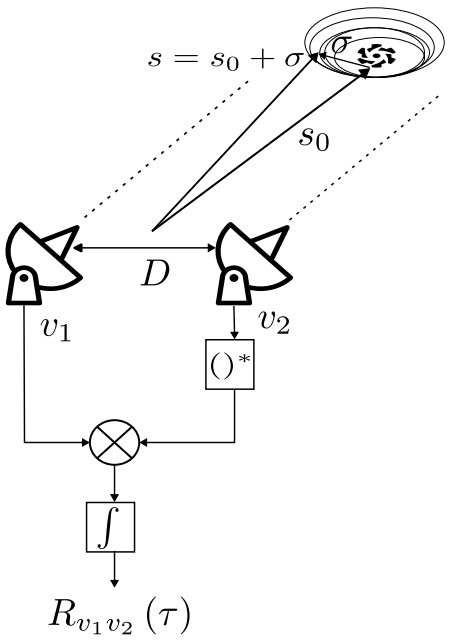

Figure 1. Cross-correlator block diagram.

$$\begin{aligned} v_{Aut}(\omega) = v_2(\omega) &= \int\limits_{source} e_{Aut}(\boldsymbol{\sigma},\omega)\, Q_2(\boldsymbol{\sigma},\omega)\, d\Omega \\ v_{Ref}(\omega) = v_1(\omega) &= \int\limits_{source} e_{Ref}(\boldsymbol{\sigma},\omega)\, Q_1(\boldsymbol{\sigma},\omega)\, d\Omega \end{aligned} \tag{4}$$

where $Q(\boldsymbol{\sigma},\omega)$ is the voltage reception pattern of the antenna.

If the radiosource is incoherent

$$\langle \widetilde{e}(\boldsymbol{\sigma},\omega)\, \tilde{e}^*(\acute{\boldsymbol{\sigma}},\acute{\omega})\rangle = 2\pi\tilde{\gamma}(\boldsymbol{\sigma}-\grave{\boldsymbol{\sigma}},\omega)\,\delta(\boldsymbol{\sigma}-\acute{\boldsymbol{\sigma}})\,\delta(\omega-\acute{\omega}) \tag{5}$$

where $\tilde{\gamma}(\boldsymbol{\sigma},\omega)$ is the Fourier transform of the self-coherence function $\gamma(\boldsymbol{\sigma},\tau) = \left\langle e(\boldsymbol{\sigma},t), e\left(\boldsymbol{\sigma},t'\right)\right\rangle$ and δ is the Dirac delta function. As the received voltages are jointly stationary processes

$$\langle \widetilde{v}_1(\omega)\, \widetilde{v}_2^*(\acute{\omega})\rangle = 2\pi S_{v_1 v_2}(\omega)\,\delta(\omega-\acute{\omega}) \tag{6}$$

then, the crosspower spectrum is

$$S_{v_1 v_2}(\omega) = \int\limits_{source} I_\nu(\boldsymbol{\sigma})\mathbf{Q_1}(\boldsymbol{\sigma},\omega)\,\mathbf{Q_2^*}(\boldsymbol{\sigma},\omega)\,\mathrm{e}^{-\mathrm{i}\omega\tau_g(\boldsymbol{\sigma})}\mathrm{d}\Omega \tag{7}$$

where $I_\nu(\boldsymbol{\sigma})$ is the source intensity distribution ($I_\nu(\boldsymbol{\sigma}) = 4\tilde{\gamma}(\boldsymbol{\sigma},\omega)$). This equation is the equivalent of power received for a single antenna

$$S_{vv}(\omega) = \int\limits_{source} I_\nu(\boldsymbol{\sigma}) \mathbf{Q}(\boldsymbol{\sigma},\omega)\, \mathbf{Q}^*(\boldsymbol{\sigma},\omega)\, \mathbf{d\Omega} \tag{8}$$

but now, with an interferometer, the cross-spectrum is influenced by the relative phase term $e^{-i\omega\tau_g(\boldsymbol{\sigma})}$.

To get the cross-correlation, the inverse Fourier transform of equation (7) is calculated

$$R_{v_1v_2}(\tau) = \frac{1}{2\pi}\int\limits_{-\infty}^{\infty} S_{v_1v_2}(\omega)\, e^{i\omega\tau} d\omega = \frac{1}{2\pi}\int\limits_{-\infty}^{\infty}\int\limits_{source} I_\nu(\boldsymbol{\sigma}) \mathbf{Q_1}(\boldsymbol{\sigma},\omega)\, \mathbf{Q_2^*}(\boldsymbol{\sigma},\omega)\, \mathrm{e}^{-\mathrm{i}\omega\tau_\mathrm{g}(\boldsymbol{\sigma})} \mathrm{d}\Omega \mathrm{d}\omega \tag{9}$$

If the source is a point source, the last equation reduces to

$$R_{v_1v_2}(\tau) = \frac{1}{2\pi}\int\limits_{-\infty}^{\infty} Q_1(\mathbf{0},\omega)\, Q_2^*(\mathbf{0},\omega)\, e^{-i\omega\tau_g(\mathbf{0})} d\omega = \rho_{v_1v_2}(\tau - \tau_g) \tag{10}$$

where $\rho_{v_1v_2}$ is the cross-correlation function of the two antennas when their relative delay is zero. In other words, the effect of the relative delay between both antennas will be a shift of τ_g samples in the correlation function.

A. Discrete Time Processing

For a white noise source that is sampled at f_s samples/second and filtered at B hertz, the resulting digital cross-correlation version of equation (9) will be

$$R_{v_1v_2}(m) = Q_1 Q_2^* B_n \,\mathrm{sinc}\left(B_n\left(m - m_g\right)\right) \tag{11}$$

where $B_n = B/(f_s/2)$ is the normalized bandwitdh, and $m_g = \tau_g/f_s$ is the delay expressed in samples. Therefore, as long as the full cross-correlation function is computed, in principle there is no need to compensate for the delay between both antennas. Just getting the peak will give us the relative phase and amplitude between both antennas. When working with noisy inputs, this procedure can only be applied as long as the peak is not far away from the center, as it will be shown next.

The computation in the GPU of the cross-correlation will be done in the frequency domain in order to take advantage of the parallelization capabilites of the GPU. First, the Fourier transforms of the signals of both antennas are computed; we divide the L samples into M periods of N samples each. For the reference antenna

$$V_1(\omega, m) = \sum_{n=0}^{N-1} v_1[n]\, e^{-i\omega n} \tag{12}$$

and for the AUT

$$V_2(\omega, m) = \sum_{k=0}^{N-1} v_2[k]\, e^{-i\omega k} \tag{13}$$

Both Fourier transforms are multiplied and averaged over M periods of N samples

$$S_{v_1 v_2}^{avg}(\omega) = \frac{1}{M} \sum_{n=0}^{M-1} V_1(\omega, m)\, V_2^*(\omega, m) \tag{14}$$

The expected average of equation (14) is described in [5]:

$$E\left[S_{v_1 v_2}^{avg}(\omega)\right] = \sum_{n=0}^{N-1} \sum_{k=0}^{N-1} E\left[v_1[n]\, v_2^*[k]\right] e^{-i\omega(n-k)} = \sum_{n=0}^{N-1} \sum_{k=0}^{N-1} R_{v_1 v_2}(n-k)\, e^{-i\omega(n-k)} \tag{15}$$

which after manipulation becomes

$$E\left[S_{v_1 v_2}^{avg}(\omega)\right] = \sum_{m=-(N-1)}^{N-1} R_{v_1 v_2}[m] \left(1 - \frac{|m|}{N}\right) e^{-i\omega m} \tag{16}$$

In other words, the expectancy of the average of the cross-product of the FFTs is the Fourier transform of the following function:

$$E\left[R_{v_1 v_2}^{avg}[m]\right] = R_{v_1 v_2}[m] \left(1 - \frac{|m|}{N}\right) \tag{17}$$

The further we compute the cross-correlation from the center ($m = 0$), the more biased the cross-corelation becomes. In order to get the relative amplitude and phase between both antennas, we divide the averaged cross-spectra by the averagec spectrogram of the reference antenna,

$$E\left[S_{v_1 v_1}^{avg}(\omega)\right] = \sum_{m=-\infty}^{\infty} R_{v_1 v_1}[m] \left(1 - \frac{|m|}{N}\right) e^{-i\omega m} \tag{18}$$

Modeling the signal as a white-noise ergodic process (as in the case of radio stars) $R_{v_1 v_1}[m] = \delta[m]$ and considering that the signal at the AUT is a delayed version of the reference antenna $v_2[m] = Ae^{i\phi} v_1[m - D]$, then

$$\frac{E\left[S^{avg}_{v_1v_2}(\omega)\right]}{E\left[S^{avg}_{v_1v_1}(\omega)\right]} = \frac{Ae^{i\phi}R_{v_1v_1}[0]\left(1-\frac{|D|}{N}\right)e^{-i\omega D}}{R_{v_1v_1}[0]} \tag{19}$$

whose inverse Fourier transform is precisely a delta at the delay D

$$F^{-1}\left(\frac{E\left[S^{avg}_{v_1v_2}(\omega)\right]}{E\left[S^{avg}_{v_1v_1}(\omega)\right]}\right) = F^{-1}\left(Ae^{i\phi}\left(1-\frac{|D|}{N}\right)e^{-i\omega D}\right) = \left(1-\frac{|D|}{N}\right)Ae^{i\phi}\delta[m-D] \tag{20}$$

The division by the average spectrogram of the reference antenna and posterior inverse transform is nothing more than the Wiener filter. In order to avoid zero divisions at some points in the spectrum, the same result can be obtained by dividing by the power of the reference antenna, i.e. $R^{avg}_{v_1v_1}[0] = \sum_{m=0}^{N-1} S^{avg}_{v_1v_1}(m)$

If we introduce thermal noise to both antennas ($x = v_1 + n_1$, $y = v_2 + n_2$), the variance of the estimation of the cross-correlation is found to be

$$V\left[R^{avg}_{xy}[m]\right] = \frac{1}{N}\sum_{n=-\infty}^{\infty} R_{xx}[n]R_{yy}[n] + R_{xy}[n-m]R_{yx}[n+m] = \frac{1}{N}\left((R_{vv}[0]+R_{nn}[0])(A^2R_{vv}[0]+R_{nn}[0]) + A^2R^2_{vv}[0]\right) \tag{21}$$

Therefore if we divide the expected cross-correlation value at its peak by its variance we get the signal-to-noise ratio of the cross-correlation

$$SNR_{XCOR} = \frac{\left(1-\frac{|D|}{N}\right)AR_{v_1v_1}[0]}{\sqrt{\frac{1}{N}\left((R_{vv}[0]+R_{nn}[0])(A^2R_{vv}[0]+R_{nn}[0]) + A^2R^2_{vv}[0]\right)}} \tag{22}$$

If the AUT is scanning a sidelobe far from the center $A \ll 1$, then the equation above can be simplified to

$$SNR_{XCOR} = \frac{\left(1-\frac{|D|}{N}\right)AR_{vv}[0]}{\sqrt{\frac{1}{N}\left((R_{vv}[0]+R_{nn}[0])(R_{nn}[0])\right)}} \approx \sqrt{N}\left(1-\frac{|D|}{N}\right)SNR \tag{23}$$

As expected, the SNR in the cross-correlation increases with the square root of the number of samples. However, if the peak of the cross-correlation is far from zero (D is large), the cross-corelation peak will be decreased by the factor $\frac{N-D}{N}$, which for large

values of D is close to zero. The explanation is simple: If the relative delay between the antennas is close to the cross-correlation window, then the averaging will be done only in a small fraction of the data window. Hence, only a few signal samples will be added up in phase. The actual implementation of the correlator takes into account this fact. Prior to the correlation, the packets are aligned using the timestamp info from the downlink telemetry and tracking subsystem (DTT). Real values of these parameters are $M = 125$ and $N = 2^{14} = 16384$. After aligning timstamps, the residual delay is no higher than 256 samples, so in the worst case the loss of SNR is less than 1%.

B. Noise Budgets

Taking into account that the number of samples acquired is $N = 2B\tau$ where B is the bandwidth and τ is the integration time, equation (23) can be written as

$$SNR_{XCOR} = \sqrt{2B\tau \frac{T_{SourceAUT} T_{SourceREF}}{T_{NoiseAUT} T_{NoiseREF}}} \tag{24}$$

where $T_{SourceAUT}$, $T_{SourceREF}$ are the source temperatures at the reference antenna and AUT, and $T_{NoiseAUT}$, $T_{NoiseREF}$ are the noise temperatures at the reference antenna and AUT. For a strong source such as 3C84, $B = 100$ MHz, $\tau = 0.2$ seconds, and 34-m antennas, the cross-correlation signal-to-noise ratio is approximately equal to 75 dB, which is good enough for performing a mid-resolution holography in 80 minutes. On the contrary, a high-resolution holography typically requires 100 dB of SNR, which cannot be accomplished with radiosources unless integration time is highly increased. With an integration time of 0.2 seconds, a high-resolution holography would take 4 hours, so increasing it further would be prohibitive. Besides, it must be taken into account that during CEI holography, the sources are moving with regards to the antenna, so the resulting phase map would be severely smeared if the total holography time exceeds 2 hours.

The other option for doing CEI holographies is using spacecrafts such as MRO or STEREO-A. Both of them provide a correlation SNR in the order of 80-90 dB, which is enough for mid-resolution holographies, but fail again for high-resolution ones. New K- and Ka-band satellites such as the James Webb Space Telescope (JWST) have wide-bandwidth signals with plenty of power. In the case of JWST ($f_c = 25.9$ GHz), the correlation SNR reaches 100 dB with an integration time of only 0.02 seconds. Under these conditions a high-resolution holography can be done in less than one hour.

The correlation SNR at boresight is related to the surface root mean square (rms) error by the following expression as described in [6]:

$$\sigma_{SNR} \approxeq 0.082 \frac{\lambda N k}{snr} \tag{25}$$

where *snr* is the voltage signal-to-noise ratio, N is the resolution grid, and k is the sampling factor ($0.5 < k < 1$; typically $k = 0.85$). As it can be observed, required SNR increases with the number of points in the grid, but also decreases for higher frequencies.

Table 1. The rms surface error in microns for $SNR = 75$ dB .

N \ frequency	X-band	Ka-band
51	24.1	7.9
127	59.9	15.9

However, for the same radiosource the flux density decreases with frequency, so the gain is not so clear. Two error budgets at X- and Ka-band are shown in Table 2

When moving to higher bands, the impact of the troposphere must be considered. Phase excursions due to the troposphere scale with frequency according to the following rule as described by [7]:

$$\phi_{f_2} = \phi_{f_1} \frac{f_2}{f_1} \tag{26}$$

However, the rms surface error decreases in the same proportion with frequency as described by [8]:

$$\sigma_\phi \approxeq \frac{\phi_{rms}\lambda}{6\pi} \Longrightarrow \sigma_{\phi_{f_2}} = \frac{\phi_{f_1}\frac{f_2}{f_1}\frac{c}{f_2}}{6\pi} = \sigma_{\phi_{f_1}} \tag{27}$$

Therefore, the accuracy in each resolution cell of the final holography maps is better at higher frequencies for the same SNR, and remains the same as we move in frequency with regards to the error introduced by the troposphere.

Table 2. The rms error budgets for mid-resolution holographies ($N = 51$, $\tau = 0.2$ seconds) in X- and Ka-bands for 3C273 and two 34-m antennas.

	X-band	Ka-band	Ka-band	Ka-band
Flux Density (Jy)	30	15	15	15
Efficiency (%)	0.7	0.5	0.5	0.5
Source Temperature (Kelvin)	13.8	4.9	4.9	4.9
Noise Temperature (Kelvin)	20	40	40	40
Bandwidth (MHz)	100	100	200	400
SNR (dB)	72.8	57.9	60.9	63.9
σ_{SNR}(microns)	27.4	40.2	28.4	20.1

The rms surface error brought about by the troposphere is very high. With a $\phi_{rms} = 5$ degrees in X-band, the accuracy in the surface map is reduced to $\sigma_\phi = 50$ microns. If no other actions are taken to mitigate this effect, CEI holographies should only be done during calm tropospheric conditions (typically at night). This is very limiting, but polar sampling schemes can be used to alleviate the impact of the troposphere as shown in [9].

C. Extended Sources

As we saw in equation (7), in the case of the interforemeter, the integration of the intensity distribution of the source is affected by the grating lobes of the interferometer. The simple case of a source with a circular Gaussian intensity distribution can be described as

$$I\left(\xi,\eta\right) = \frac{S_T}{\pi\Theta^2{}_s} e^{-\frac{\xi^2+\eta^2}{\Theta^2{}_s}} \tag{28}$$

where S_t is the total flux density, and Θ_s is the source size. If the antenna patterns of the antennas do not resolve the source, [4] demonstrates it can be shown that

$$S_{v_1 v_2}\left(\omega\right) = \int\limits_{source} I_\nu(\boldsymbol{\sigma})\mathbf{Q_1}\left(\boldsymbol{\sigma},\omega\right)\mathbf{Q_2^*}\left(\boldsymbol{\sigma},\omega\right)\mathrm{e}^{-\mathrm{i}\omega\tau_\mathrm{g}(\boldsymbol{\sigma})}\mathrm{d}\Omega = \mathrm{S_t e}^{-\left[\Theta_s\omega\frac{\mathrm{D}\cos\theta}{2\mathrm{c}}\right]^2} \tag{29}$$

where $D\cos\theta$ is the projected baseline. This means that the power is reduced by half when the half power width distribution of the source θ_0 is equal to

$$\theta_0 \cong 0.44\frac{\lambda}{D\cos\theta} \tag{30}$$

Table 3. Source half power width for 3dB loss at the output of the correlator.

frequency / Baseline	X-band	Ka-band
1 Kilometer	3.2 arcseconds	850 milliarcseconds
10 Kilometers	320 milliarcseconds	85 milliarcseconds

3C84, 3C273, 3C279, and 3C454.3 are strong sources with widths on the order of a few milliarcseconds [10], so they can be used without problems at any of the DSN centers. 3C274 has an extension of a few arcminutes so it should be avoided.

D. Bandwidth Integration

Let's downconvert the received signal to baseband. The resulting expression for the crosspower spectrum is

$$S_{v_1 v_2}^{bb}(\omega) = S_{bb}(\omega)\, e^{-i\omega\tau_g(\boldsymbol{\sigma_s})} Q_1(\boldsymbol{\sigma_s}, \omega+\omega_c)\, Q_2^*(\boldsymbol{\sigma_s}+\boldsymbol{\sigma_0}, \omega+\omega_c)\, \mathrm{e}^{-\mathrm{i}\omega_c\tau_g(\boldsymbol{\sigma_s})} \quad (31)$$

The first thing to do is to compensate for the relative Doppler between both antennas by multipliying the signal at the AUT by the factor $e^{i\omega_c\tau_g(\boldsymbol{\sigma_s})}$. Now, suppose that a puntual source is received (no need for source angular integration), and that the delay between both antennas is compensated $\tau_g(\boldsymbol{\sigma_s}) = 0$. Assume also a flat passband that extends $\omega_B/(2\pi)$ hertz ($S_{bb}(\omega) = 1$ if $|\omega| < \omega_B/2$). If the reference antenna is pointing at all time at the source, it can be assumed that $Q_1(\boldsymbol{\sigma_s}, \omega+\omega_c) = 1$. Now move the AUT an angle θ away from boresight. Assuming a circular uniform aperture $Q_2(\boldsymbol{\sigma_s}+\boldsymbol{\sigma_0}, \omega+\omega_c) = Ae^{i\phi}\frac{J_1\left(\frac{\omega}{c}a\sin(\theta)\right)}{\frac{\omega}{c}a\sin(\theta)}$, where A and ϕ are some constant amplitude and phase. The beam pattern of the AUT changes with frequency as shown in Figure 2.

Figure 2 shows that the further we are from the central frequency, the more squint in the sidelobes. This tendency is also exacerbated with the angular distance to the boresight. The same happens in the phase of the radiation pattern (Figure 3)

This fact has an impact in the cross-correlator output, as all of the frequencies within the integration bandwidth are accounted for. The resulting output can be computed by inserting the radiation pattern of the AUT into equation (9)

$$R_{v_1 v_2}^{bb}(\tau) = \int_{-\infty}^{\infty} \prod\left(\frac{\omega}{\omega_B}\right) Q_1(\boldsymbol{\sigma_s}, \omega+\omega_c)\, Q_2^*(\boldsymbol{\sigma_s}, \omega+\omega_c)\, e^{i\omega t} d\omega = \int_{-\infty}^{\infty} \prod\left(\frac{\omega}{\omega_B}\right) \left(Ae^{i\phi}\frac{J_1\left(\frac{(\omega+\omega_c)}{c}a\sin(\theta)\right)}{\frac{(\omega+\omega_c)}{c}a\sin(\theta)}\right)^* e^{i\omega\tau} d\omega \quad (32)$$

As the delay is compensated (or the cross-correlation is evaluated at the exact relative delay), then the value to look for in the cross-correlation is the one at the peak, i.e., $B = 8.45$ GHz

$$R_{v_1 v_2}^{bb}(0) = \int_{-\omega_B/2}^{\omega_B/2} \left(Ae^{i\phi}\frac{J_1\left(\frac{(\omega+\omega_c)}{c}a\sin(\theta)\right)}{\frac{(\omega+\omega_c)}{c}a\sin(\theta)}\right) d\omega \quad (33)$$

Equation (33) shows that the beam pattern is the result of averaging the beam patterns at all frequencies included in the bandwidth of the received signal. The result

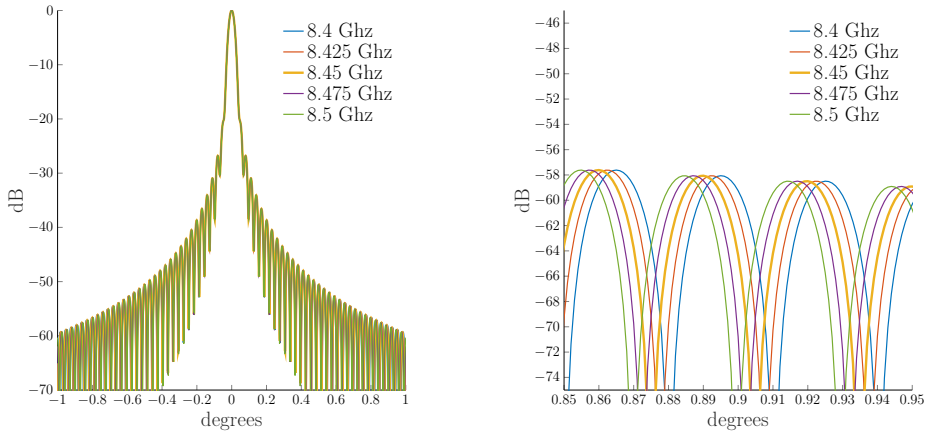

(a) Complete **(b) Zoom**

Figure 2. Amplitude pattern of a TE_{11} mode circular distribution aperture on ground plane at different central frequencies.

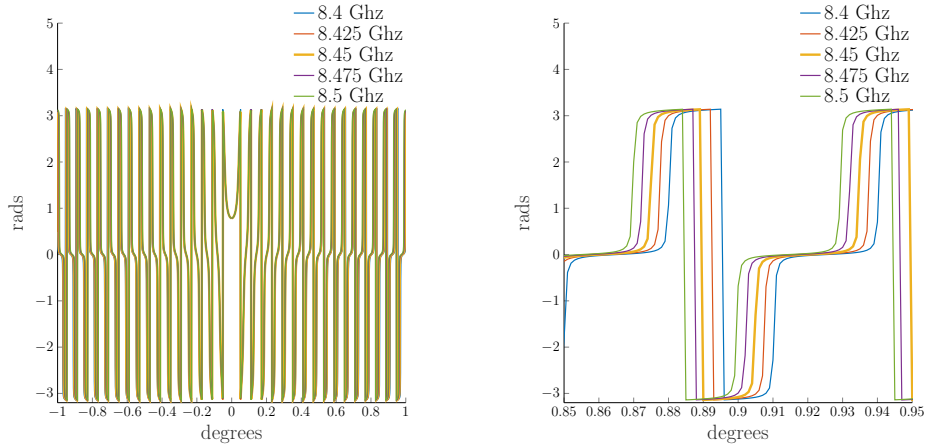

(a) Complete **(b) Zoom**

Figure 3. Phase pattern of a TE_{11} mode circular distribution aperture on ground plane at different central frequencies.

of this integration is shown in Figures 4 and 5. When integrating 100 MHz in X-band, the peak of the sidelobes is decreased by up to 1 dB in the farthest sidelobes, but the phase remains nearly the same. Amplitude losses have been quantified for several integration bandwidths as shown in Figure 6. In Ka-band, bandwidths of 400 MHz can be used with even a lower degradation than 100 MHz in X-band. With 400 MHz the correlation SNR (equation (24)) is increased by 3 dB with regards to 100 MHz; however, the same source in Ka-band usually has a lower flux density, so, in all, the correlation SNR remains approximately the same. As shown in Table 1, with the same SNR, a higher frequency band means lower rms surface error, so doing a mid-resolution holography in Ka-band with 400 MHz bandwidth would decrease the rms surface error by a factor of 3 in comparison with a mid-resolution holography in X-band with 100 MHz for the same source.

III. HW & SW Implementation

As mentioned in the introduction, a 100 MHz cross-correlator has been implemented in a workstation with most of the heavy signal processing done in a Nvidia GPU (RTX 3090 or RTX 6000 ADA). Figure 7 shows the data flow from the samples distributed by the Common Platform to the final amplitude/phase measurement. First, for each antenna, 16 subbands coming from 8 UDP multicasts are acquired by the Mellanox card in segments of .16 seconds (a total of 2048 frames of 80 microseconds for each one). This accounts for a total of 16 Mega complex samples that are processed as a whole by the subsequent stages. In the first stage, the timestamps of the different subbands are extracted in the CPU, and used by a Sync algorithm to align at frame level all subbands. After synchronization of the frames, the samples are sent to the GPU.

Processing in the GPU is done using Compute Unified Device Architecture (CUDA) and ArrayFire [11]. The first operation in the GPU is the filterbank synthesis. A 16-point decimation in time FFT has been coded in ArrayFire with input vectors of 1 Mega complex samples. Afterwards, timestamps are used to compensate the time delay betweeen two antennas, leaving a residual offset lower than 200 samples ($<$1% frame time). In cases where the signal is coming from a spacecraft, a tunable variable filter gets rid of excess noise around it. Then, differential Doppler is compensated in the antenna under test. Next, the cross-correlation is computed by using the frequency domain algorithm in [12]. To increase the accuracy in the amplitude and phase estimations, the resulting correlation is interpolated by a factor of 32. When the antenna is scanning far away from the main lobe, the peak of the cross-correlation function is buried under noise. Under these circumstances, predicts are used to correctly track the peak of the correlation function. All processing requires roughly 0.5 teraops/second (FP32), with less than 4 GB of GPU RAM used.

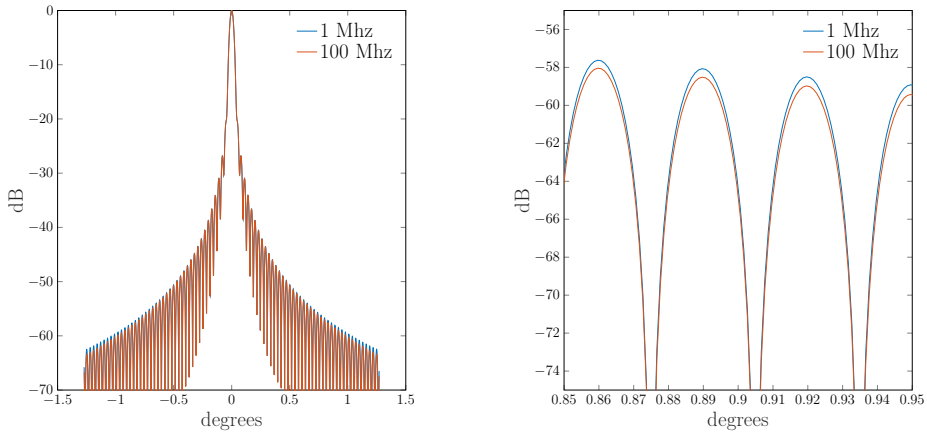

(a) Complete **(b) Zoom**

Figure 4. Amplitude pattern of a TE_{11} mode circular distribution aperture on ground plane with $f_c = 8.45$ GHz and different integration bandwidths.

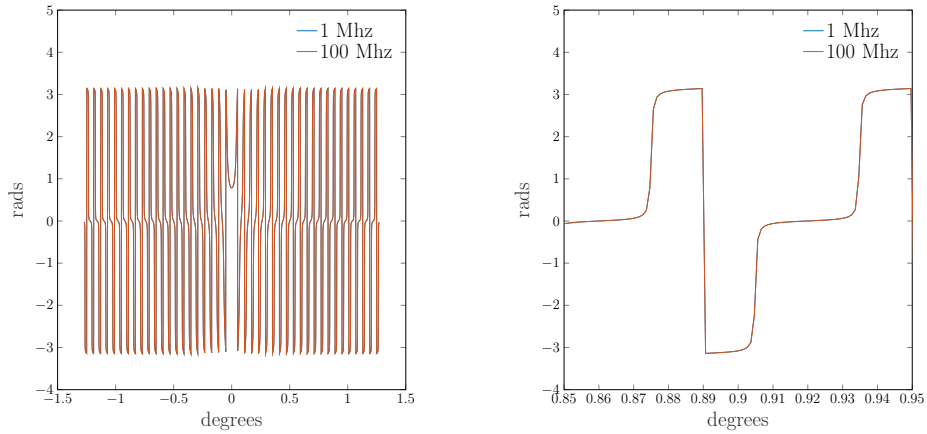

(a) Complete **(b) Zoom**

Figure 5. Phase pattern of a TE_{11} mode circular distribution aperture on ground plane with $f_c = 8.45$ GHz and different integration bandwidths.

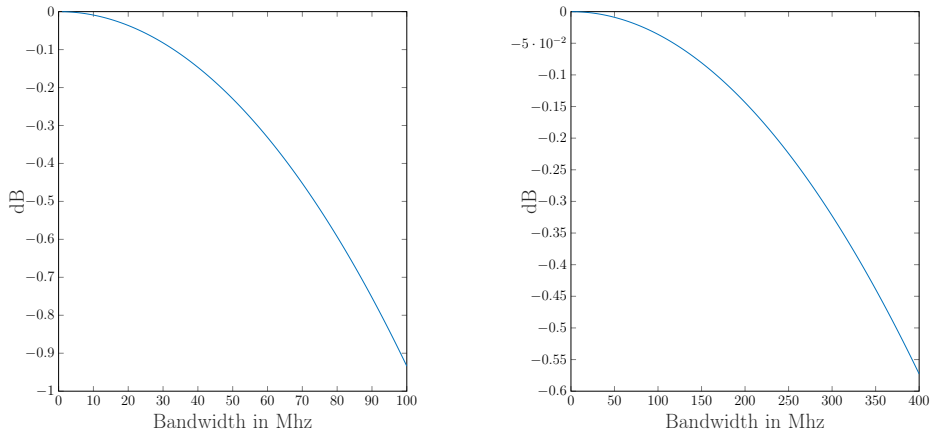

(a) X-band **(b) Ka-band**

Figure 6. Bandwidth integration losses for a circular aperture.

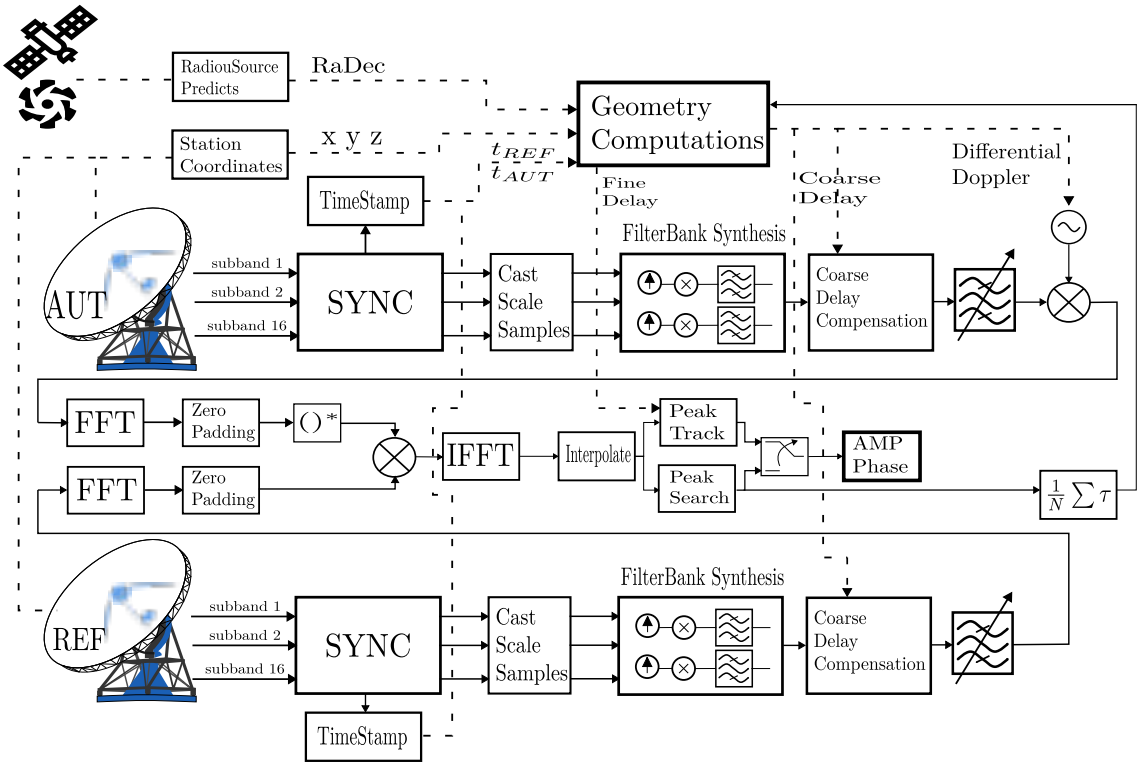

Figure 7. Signal processing scheme.

IV. Measurements

CEI holographies have been tested during 2022 and 2023 at MDSCC with good results. In 2023, CEI holographies were used to align microwave mirrors in DSS-55; several radiosources were used, mainly 3C273, 3C84, MRO, and STEREO-A . Also, in 2023, an holography campaign was done with DSS-63 to assess the status of the dish. During this campaign, gravity deformation of the dish was measured. To do so, DSS-54 was used as a refererence antenna and radiosource 3C84 was followed for several hours at night while it went from low to high elevation. Every 1 hour, a mid-resolution holography was done. At the end, the resulting maps were compared with the map at the rigging angle (45 degrees). The results in Figures 8 and 9 show how the antenna deforms due to gravity load; the measured deformation fits the expected finite element model in [13]. The computed antenna directivity from these illumination maps is shown in Figure 10.

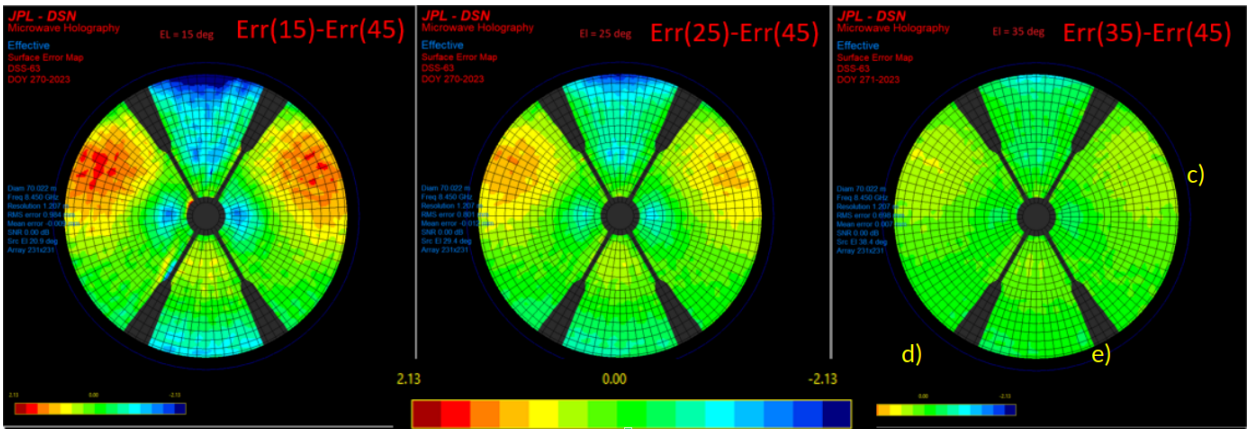

Figure 8. DSS-63 low-elevation holographies.

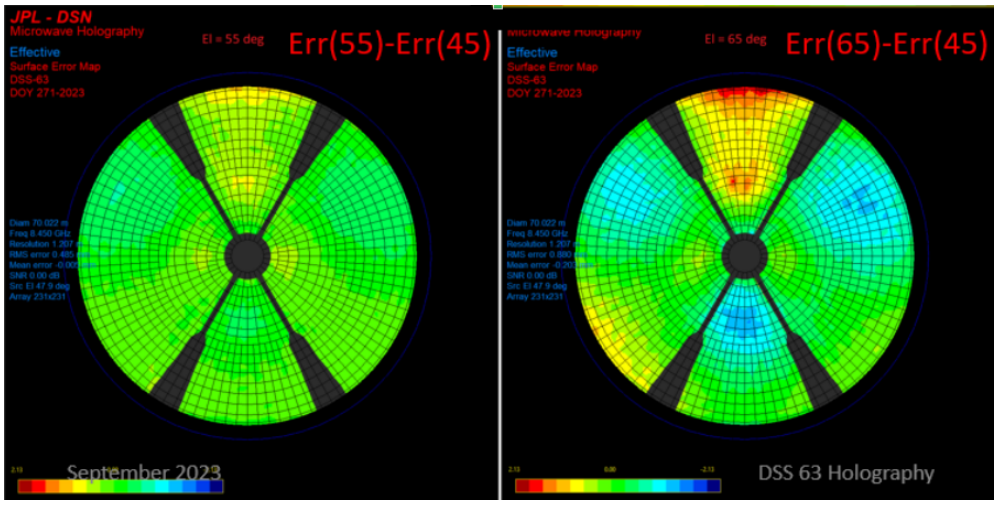

Figure 9. DSS-63 high-elevation holographies.

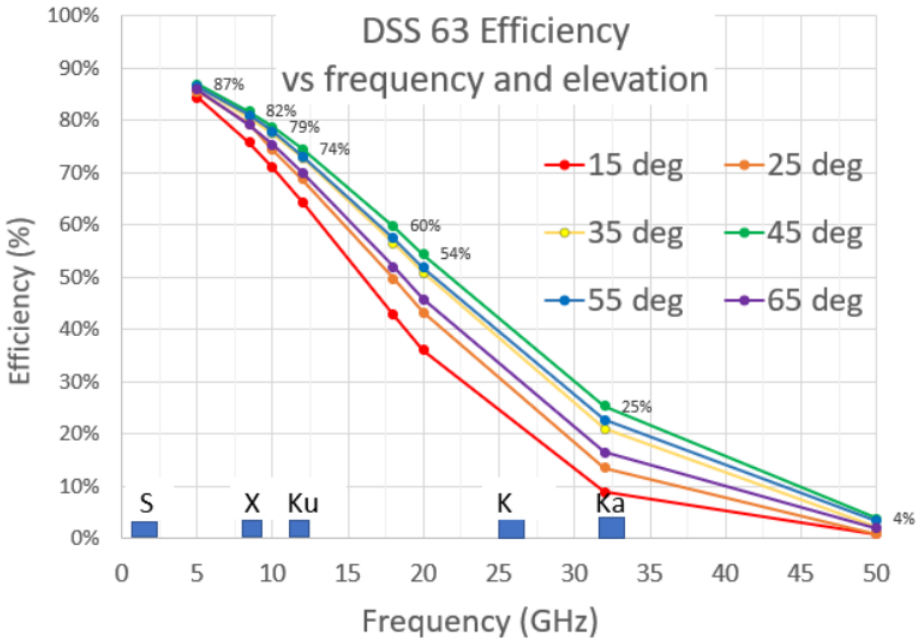

Figure 10. DSS-63 efficiency.

References

[1] D. J. Rochblatt, "A microwave holography methodology for diagnostics and performance improvement for large reflector antennas," *The Telecommunications and Data Acquisition Progress Report*, vol. 42-108, Jet Propulsion Laboratory, Pasadena, California, pp. 235–252, Feb. 1992.

[2] Y. Rahmat-Samii, S. Gulkis, B. L. Seidel, L. Young, M. Batty, and D. L. Jauncey, "Microwave holographic surface measurement of the Tidbinbilla 64-m antenna," *Proceedings of the Astronomical Society of Australia*, vol. 5, no. 219, 1983.

[3] A. Jongeling and R. Navarro, "A Common Platform for DSN receiver development," *IEEE Aerospace Conference, Big Sky, Montana*, 2019.

[4] T. Sasao and A. B. Fletcher, *Introduction to VLBI Systems*. Lecture notes for KVN students, 2005.

[5] J. Larsen, "Correlation functions and power spectra," tech. rep., Technical University of Denmark, 2009.

[6] D. J. Rochblatt and B. L. Seidel, "Microwave antenna holography," *IEEE Transactions on Microwave Theory and Techniques*, vol. 40, no. 6, 1992.

[7] M. J. Zemba, J. R. Morse, and J. A. Nessel, "Ka-band atmospheric phase stability measurements in Goldstone, CA; White Sands, NM; and Guam," *The 8th European Conference on Antennas and Propagation (EuCAP 2014)*, The Hague, Netherlands, 2014.

[8] B. Butler, "Simulations of some types of holography errors for VLBA antennas," tech. rep., National Radio Astronomy Observatory, 1999.

[9] A. Torre and M. Vazquez, "Connected-element interferometry holography with polar sampling," *The Interplanetary Network Progress Report*, vol. 42-241, Jet Propulsion Laboratory, Pasadena, California, pp. 1–18, 2025.

[10] Y. Koyama and T. Kondo, "Microwave flux density variations of compact radio sources monitored by real-time very long baseline interferometry," *Radio Science*, vol. 36, no. 2, pp. 223–235, 2001.

[11] P. Yalamanchili, U. Arshad, Z. Mohammed, P. Garigipati, P. Entschev, B. Kloppenborg, J. Malcolm, and J. Melonakos, "ArrayFire - A high performance software library for parallel computing with an easy-to-use API," AccelerEyes, Atlanta, Georgia, 2015.

[12] S. L. Marple, "Estimating group delay and phase delay via discrete-time "analytic" cross-correlation," *IEEE Transactions on Signal Processing*, vol. 47, no. 9, 1999.

[13] D. J. Rochblatt, D. J. Hoppe, W. A. Imbriale, M. M. Franco, P. H. Richter, P. M. Withington, and H. J. Jackson, "A methodology for the open loop calibration of a

deformable flat plate on a 70 meter antenna," *Millenium Conference on Antennas and Propagation, Davos, Switzerland*, 2000.